

Testing the Star-disk Collision Model for Quasi-periodic Eruptions

WENYUAN GUO (郭文渊) ^{1,2} AND RONG-FENG SHEN (申荣锋) ^{1,2}

¹*School of Physics and Astronomy, Sun Yat-sen University, Zhuhai 519082, China*

²*CSST Science Center for the Guangdong-Hong Kong-Macau Greater Bay Area, Sun Yat-sen University, Zhuhai 519082, China*

ABSTRACT

Quasi-periodic eruptions (QPEs), the repeated outbursts observed in soft X-ray bands, have attracted broad interest, but their physical origin is under debate. One of the popular models, the star-disk collision model, suggests that QPEs can be produced through periodic collisions of an orbiting star with the accretion disk of a central black hole (BH). However, previous tests of the star-disk collision model mainly focus on the timing analysis. Other observed properties, such as peak luminosities L_p , durations t_e , and radiation temperatures T_p of the eruptions, are not systematically investigated. For a sample of six QPE sources and two QPE-like sources, we test the star-disk collision model by using these observables to derive the constraints on the stellar radius R_* . We find that, except for two sources (eRo-QPE3 and eRo-QPE4), the rest of the sample either has no allowed R_* to simultaneously reproduce the observed L_p and t_e , or the required R_* is too large to avoid being disrupted by the central BH. For the two exceptions, a stellar radius of the order of $1 R_\odot$ is necessary to satisfy all the constraints. Another issue with the simplest version of this model is that it predicts $kT_p \sim 10$ eV, one order of magnitude lower than the observed value.

Keywords: X-ray transient sources (1852) — Tidal disruption (1696) — Supermassive black holes (1663)

1. INTRODUCTION

The probe of massive BHs is one of the most attractive subjects in astrophysics. This helps answer whether there is at least a supermassive BH (SMBH) located in each galaxy's center. Past efforts to investigate the population of SMBHs have been based on observing the orbital motion of surrounding stars or some BH-accretion-related high-energy phenomena. In the near future, gravitational wave detectors have the potential to detect SMBHs in binary systems.

Recently, a new class of repeating soft X-ray outbursts called quasi-periodic eruptions (QPEs) have been discovered. Motivated by the first reported QPE, GSN 069 (Miniutti et al. 2019, 2023a,b), RX J1301 and eRo-QPE1-4 are discovered (Sun et al. 2013; Giustini et al. 2020; Arcodia et al. 2021, 2024a,b; Chakraborty et al. 2024). They exhibit luminous flares with the peak luminosity of $L_p \approx 10^{42}$ erg/s, the duration of $t_e \approx 1$ hr, and recurring over a period of $P \approx 10$ hr. Based on the fitting of the spectrum, their peak temperature $kT_p \approx 100$ eV. They are located at the nuclei

of their host galaxies with a quiescent luminosity of $L_Q \approx 10^{41}$ erg/s, thus potentially linked to a massive BH with the mass of $M_h \approx 10^6 M_\odot$. Also, due to periodic behaviors, QPE-like events like ASASSIN14-ko and Swift J0230 (hereafter called J0230 for short) (Payne et al. 2021, 2022, 2023; Huang et al. 2023; Linial & Quataert 2024; Evans et al. 2023; Guolo et al. 2024) are expected to originate from the same physical process as QPEs.

On the basis of observations, several theoretical models have been proposed to interpret QPEs. Generally, they can be classified into four kinds: 1) disk instability model (Raj et al. 2021; Pan et al. 2022; Kaur et al. 2023; Śniegowska et al. 2023), 2) self-lensing model in massive BH binary (Ingram et al. 2021), 3) star-disk collision model (Dai et al. 2010; Pihajoki 2016; Suková et al. 2021; Xian et al. 2021; Franchini et al. 2023; Linial & Metzger 2023; Linial & Quataert 2024; Tagawa & Haiman 2023), 4) mass transfer model between a stellar companion and the SMBH, such as via Roche lobe overflow (Metzger et al. 2022; Linial & Sari 2023), repeated tidal stripping (King 2020, 2022, 2023; Zhao et al. 2022; Chen et al. 2023; Wu et al. 2024), stream-stream collision induced

by mass transfer (Krolik & Linial 2022; Lu & Quataert 2023). Here we focus on the star-disk collision model.

For a star orbiting around the SMBH with an accretion disk, the star will keep colliding with a disk at the crossing points between the misaligned orbit and the disk plane. The flare comes out of the ejecta shocked by the collision. Dai et al. (2010) first investigated the star-disk collision model and built a connection between the quasi-periodic behavior of flares and the star's orbital parameters. After the discovery of GSN 069 (Miniutti et al. 2019), the star-disk collision model was applied to interpret the QPEs. Several works have been dedicated to the timing analysis of QPE (Xian et al. 2021; Franchini et al. 2023; Linial & Metzger 2023; Chakraborty et al. 2024; Zhou et al. 2024a,c,b; Miniutti et al. 2025), which aims to reproduce the high-low peak luminosity pattern and the long-short pattern of QPE by various precessions.

Besides timing, the observed radiative property is also important for testing the model. Linial & Metzger (2023) studied the X-ray emission of the star-disk collision model by estimating L_p , T_p , t_e and other observation properties. However, the star-disk collision model is still not fully constrained under the observation data. For example, it is difficult to find a satisfactory quiescent-level mass accretion rate to reproduce the observed L_p , T_p and t_e simultaneously (Linial & Metzger 2023). Several simulations try to figure out the details of the star-disk collision model (Vurm et al. 2024; Yao et al. 2025).

In this paper, we carefully check the estimations in Linial & Metzger (2023) and try to obtain a more holistic constraint on the star-disk collision model based on various observations of QPEs and QPE-like events. §2 present a sample of QPE and QPE-like events to be used for the test. The theoretical framework of the star-disk collision model and the test method we apply are presented in §3, and the results are given in §4. Finally, we draw our conclusions in §5.

2. THE SAMPLE OF QPE AND QPE-LIKE EVENTS

QPE and QPE-like events are outstanding for their luminous flares with repeated pulse-like light curve profiles. In this section, we summarize these observed properties of QPE and QPE-like events, which are used in the constraints of r_* .

GSN 069 shows a sequence of soft X-ray eruptions lasting for $t_e \approx 1.1$ hr with $P \approx 8.5$ hr and $L_p \approx (10^{42} - 10^{43})$ erg/s (Miniutti et al. 2019, 2023b,a). Between eruptions, $L_Q = (2 - 3) \times 10^{43}$ erg/s (Miniutti et al. 2019, 2023b). Fitting by the Planck function,

$kT_p \approx (70 - 120)$ eV (Miniutti et al. 2019, 2023b,a). Based on the DISKBB model fitting, Miniutti et al. (2019, 2023b,a) inferred $M_h \approx (2 - 4) \times 10^6 M_\odot$.

RX J1301 has shown three rapid flares in 2019 and one flare in 2000. These flares last for $t_e = (1 - 2)$ ks with $L_p \approx 10^{42}$ erg/s and $P = 17$ ks (Giustini et al. 2020). During the quiescent state, $L_Q = (0.3 - 2) \times 10^{41}$ erg/s. (Sun et al. 2013; Giustini et al. 2020) Based on diskbb or bbody models with serious components, $kT_p = (94 - 330)$ eV (Sun et al. 2013; Giustini et al. 2020). The mass of BH inferred from the UV/X-ray analysis is $M_h = (8 - 28) \times 10^5 M_\odot$ (Sun et al. 2013).

eRo-QPE1 is first reported for its luminous flares lasting for $t_e = (6.6 - 8.6)$ hr with $P = 18$ hr (Arcodia et al. 2021) and the later 3.5 yr monitoring presented by Chakraborty et al. (2024) shows its large variation in light curve. Generally, its various flares peak with $L_p = (8 - 200) \times 10^{41}$ erg/s and $L_Q = (1 - 6.6) \times 10^{40}$ erg/s (Arcodia et al. 2021; Chakraborty et al. 2024). eRo-QPE2 is also reported by Arcodia et al. (2021); Pasham et al. (2024b); Arcodia et al. (2024a) as a luminous QPE source with $P = 2.4$ hr. It rises to a high state for $t_e = (24 - 30)$ min with $L_p = (0.1 - 1.2) \times 10^{42}$ erg/s (Arcodia et al. 2021; Pasham et al. 2024b; Arcodia et al. 2024a). In the quiescent state, $L_Q = 4 \times 10^{40}$ erg/s (Arcodia et al. 2021; Pasham et al. 2024b). For these two events, inferred by the zbody, diskbb and ttabs \times zbody models, $kT_p = (85 - 200)$ eV for eRo-QPE1 (Arcodia et al. 2021; Chakraborty et al. 2024) and $kT_p = (150 - 240)$ eV for eRo-QPE2 (Arcodia et al. 2021; Pasham et al. 2024b; Arcodia et al. 2024a). Next, based on disk luminosity, duration, and period with adopting different viscosity parameters α , $M_h = (60 - 4 \times 10^6) M_\odot$ for eRo-QPE1 and $M_h = (300 - 3 \times 10^6) M_\odot$ for eRo-QPE2 (Arcodia et al. 2021; Pasham et al. 2024b; Arcodia et al. 2024a).

eRo-QPE3 and eRo-QPE4 are reported by Arcodia et al. (2024b). Based on observations, eRo-QPE3 peaks with $L_p = (0.4 - 1) \times 10^{42}$ erg/s with $P = 20$ hr and $L_Q = 1.6 \times 10^{40}$ erg/s (Arcodia et al. 2024b). For eRo-QPE4, the eruptions repeated every 14 hr with $L_p = (4 - 15) \times 10^{42}$ erg/s and $L_Q = (10^{41} - 10^{43})$ erg/s (Arcodia et al. 2024b). With assumption of a Gaussian light curve profile, $t_e = (2 - 2.7)$ hr for eRo-QPE3 and $t_e = 1$ hr for eRo-QPE4 (Arcodia et al. 2024b). Also, fitting by a diskbb+pl model, $kT_p = (70 - 140)$ eV for eRo-QPE3 and $kT_p = (79 - 127)$ eV for eRo-QPE4 (Arcodia et al. 2024b). Moreover, inferring by the galaxy scaling relations, $M_h = (4.6 \times 10^5 - 4 \times 10^7) M_\odot$ for eRo-QPE3 and $M_h = (1.3 \times 10^7 - 1.2 \times 10^8) M_\odot$ for eRo-QPE4 (Arcodia et al. 2024b).

event	P	L_p (10^{42} erg/s)		t_e		L_Q (10^{41} erg/s)		kT_p (eV)	M_6
		range	typical value	range	typical value	range	typical value		
GSN 069 ^a	8.6 hr	1-5	3	(0.7-1.2) hr	0.94 hr	200-300	250	70-120	0.3-4
RX J1301 ^b	4.7 hr	1-3	1.0	(0.3-0.5) hr	0.4 hr	0.3-2	0.6	94-330	0.8-2.8
eRO-QPE1 ^c	18 hr	0.37-43	4.0	(6.6-8.6) hr	7.5 hr	0.10 – 0.66	0.38	85-200	6×10^{-5} -4
eRO-QPE2 ^d	2.4 hr	0.1-1.2	0.35	(0.4-0.5) hr	0.45 hr	–	0.4	150-240	3×10^{-5} -3
eRO-QPE3 ^e	20 hr	0.4-1	0.6	(2 – 2.7) hr	2.3 hr	0.2-30	2.5	70-140	0.46-40
eRO-QPE4 ^f	14 hr	4-15	7.9	(0.9 – 1.1) hr	1 hr	1-100	10	79-127	13-120
ASASSN-14ko ^g	115 days	12-200	50	(10-36) days	23 days	20-200	63	0.3-2.5	12 – 159
J0230 ^h	22 days	0.7-6	2	(2.4-6.5) days	4 days	1-2	1.5	150-200	1.5 – 10

Table 1. The observed quantities regarding the radiation properties (P , t_e , L_p , L_Q and kT_p) and the black hole masses M_h for a sample of QPEs and QPE-like events. The symbols in Ref. column are: a: Miniutti et al. (2019, 2023b,a), b: Sun et al. (2013); Giustini et al. (2020), c: Arcodia et al. (2021); Chakraborty et al. (2024), d: Arcodia et al. (2021); Pasham et al. (2024b); Arcodia et al. (2024a), e: Arcodia et al. (2024b), f: Arcodia et al. (2024b), g: Payne et al. (2021, 2022, 2023); Huang et al. (2023); Linal & Quataert (2024), h: Evans et al. (2023); Guolo et al. (2024).

Similar to QPEs, ASASSN-14ko, belonging to a subset called repeated optical nuclear transients (RNOTs), is a famous QPE-like event. It shows repeated optical flares with $P \approx 115$ days in the nuclear of the galaxy (Payne et al. 2021). The flares last for $t_e = (10 - 36)$ days with $L_p \approx (0.3 - 10) \times 10^{44}$ erg/s (Payne et al. 2021, 2022, 2023; Huang et al. 2023). Based on the relations between $M_{\text{bulge}} - M_{\text{BH}}$ and 2MASS photometry, Payne et al. (2021) obtained $M_h \approx 7 \times 10^7 M_\odot$. Using the blackbody model, $kT_p = (0.3 - 2.5)$ eV (Payne et al. 2021). The quiescent luminosity is $L_Q = 2 \times 10^{42-43}$ erg/s (Payne et al. 2021, 2022; Linal & Quataert 2024).

Furthermore, J0230 is another QPE-like source in the X-ray band with $P \approx 22$ days (Evans et al. 2023; Guolo et al. 2024). Its period is much longer than that of QPE but shorter than that of RNOT. Based on observations. It peaks with $L_p \approx 10^{42}$ erg/s and $t_e = (2.4 - 6.5)$ days (Evans et al. 2023; Guolo et al. 2024) and its $L_Q = (1 - 2) \times 10^{41}$ erg/s (Evans et al. 2023). Except for the peculiar period of flares, its $kT_p = 150 - 200$ eV and the mass of BH inferred from the $M_h - \sigma_*$ scaling relation is about $(1.5 \times 10^6 - 1 \times 10^7) M_\odot$ (Guolo et al. 2024).

In Table 1, we collect several observable properties (P , t_e , L_p , L_Q and kT_p) for a sample of QPEs and QPE-like events and their host galaxies' central BH mass M_h estimated in the literature. For QPE sources that have been monitored for long-time coverage, the three most important observables (t_e , L_p and L_Q) usually vary from eruption to eruption, therefore their observed values each have a range. In order to simplify our analysis, we will use typical values for these observables.

3. CONSTRAINTS FOR THE MODEL

Following each star-disk collision, the shocked material is brought out of the accretion disk, and then it

will experience adiabatic expansion and cooling until the matter becomes mildly optically thin, after which the radiation trapped in the shocked matter can escape. If the star is moving in an orbit with a mild eccentricity, the star will collide with the disk twice in one orbital period.

Based on the Kepler third law, assuming that the stellar orbit is near-circular, one can write disk radius R at the collision point as

$$R = \left[GM_h \left(\frac{P}{2\pi} \right)^2 \right]^{\frac{1}{3}} = 110 P_1^{\frac{2}{3}} M_6^{-\frac{2}{3}} R_g, \quad (1)$$

where $R_g = \frac{GM_h}{c^2}$ is the gravitational radius of the BH and c is the speed of light in vacuum. In order to simplify the derivation, we define the following notation: $r_* = R_*/R_\odot$, $M_6 = M_h/10^6 M_\odot$, $P_1 = P_{\text{orb}}/10$ hr and $\alpha_{-1} = \alpha/0.1$, where R_\odot and M_\odot are the solar radius and mass, α is the dimensionless disk viscosity parameter and R_* is the radius of the star.

3.1. The Disk

The disk middle plane speed of sound is $c_s = \left(\frac{\partial P}{\partial \rho} \right)^{\frac{1}{2}} = \left(\gamma \frac{P}{\rho} \right)^{\frac{1}{2}}$, where γ is the adiabatic index, ρ is the density, and pressure $P = P_{\text{gas}} + P_{\text{rad}}$ is the combination of the gas pressure P_{gas} and the radiation pressure P_{rad} . Here, we assume that the gas obeys the polytropic relation $P \propto \rho^\gamma$.

For the inner region of the disk where it is radiation-pressure and radiative-cooling dominated, the scale height of the disk is given by (also see Frank et al. 2002; Linal & Metzger 2023),

$$h = R \frac{c_s}{v_k} \simeq \frac{3\kappa \dot{M}}{8\pi c} \left[1 - \left(\frac{2R_g}{R} \right)^{\frac{1}{2}} \right] \approx 1.5 \dot{m} R_g, \quad (2)$$

where v_k is the Kepler velocity at radius R , κ is the opacity, \dot{M} is the mass accretion rate at the collision point. Hereafter we consider that the opacity is dominated by Thompson scattering, thus $\kappa = 0.34 \text{ cm}^2 \text{ g}^{-1}$. The last step of the above was used $R \gg 2R_g$. Thus, the viscosity can be expressed as $\nu \approx \alpha \sqrt{GM\dot{R}} \left(\frac{h}{R}\right)^2$. Furthermore, we use the lowercase letter $\dot{m} \equiv \dot{M}/(L_{\text{Edd}}/c^2)$ to denote the dimensionless accretion rate, where L_{Edd} is the Eddington luminosity. Under this definition, the luminosity created by accretion is $L = \eta \dot{m} L_{\text{Edd}}$, where η is the radiation efficiency.

Based on the α -disk model (Shakura & Sunyaev 1973), the surface density is given as

$$\Sigma_{\text{d}} = \frac{\dot{M}}{3\pi\nu} = 2 \times 10^4 \frac{P_1}{\alpha_{-1} \dot{m} M_6} \text{ g/cm}^2, \quad (3)$$

where $\nu \approx \alpha c_s h$ is the viscosity of the disk.

Then, the mass of shocked matter per collision is expressed as

$$\begin{aligned} M_{\text{sh}} &= 2\pi R_*^2 \left(\sqrt{2}\Sigma_{\text{d}}\right) \\ &= 4.3 \times 10^{-7} r_*^2 \frac{P_1}{\alpha_{-1} \dot{m} M_6} M_{\odot}. \end{aligned} \quad (4)$$

The factor of $\sqrt{2}$ comes from the consideration that the velocity of the disk material is perpendicular to the stellar velocity and both are of the order of to the Kepler velocity $v_k = \sqrt{\frac{GM_{\text{h}}}{R}}$, so the effective length of the stellar trajectory is $2\sqrt{2}h$.

3.2. Hydrodynamics in Collision

In the reference frame of the star, the relative velocity of the disk material is $\sqrt{2}v_k$. Assuming all the kinetic energy of the unshocked matter is converted into the internal energy of the shocked one, the internal energy per unit mass of the shocked material is

$$\epsilon_{\text{sh}}/\rho_{\text{sh}} = v_k^2, \quad (5)$$

where ϵ_{sh} and ρ_{sh} are the internal energy density and the mass density of the shocked matter, respectively.

Taking into account $\gamma = \frac{4}{3}$ and the relation $P = (\gamma - 1)\epsilon$, the speed of sound of the immediately post-shock material is

$$c_{\text{s},0} = \sqrt{\gamma \frac{P_{\text{sh}}}{\rho_{\text{sh}}}} = \frac{2}{3} v_k, \quad (6)$$

where P_{sh} is the pressure of the shocked matter. After a quasi-spherical adiabatic expansion, the terminal expansion speed of the entire shocked material would be $v_{\text{ej}} \approx c_{\text{s},0}$.

3.3. Duration of Emission

By analogy to the supernova explosion, the duration of each eruption can be estimated by the time the optical depth of the shocked matter $\tau = \kappa\Sigma$ drops to the critical value of c/v_{ej} (Arnett 1980). Then, most of the photons will escape from the shocked matter. This corresponds to when the flare reaches its peak luminosity. Hence, $\kappa\Sigma = c/v_{\text{ej}}$, where

$$\Sigma = \frac{M_{\text{diff}}}{4\pi R_{\text{diff}}^2} \quad (7)$$

is the surface density of the fireball, $R_{\text{diff}} = v_{\text{ej}}t_e$ is the radius of the fireball at its peak and t_e is the duration of the eruption. Therefore, one has (also see Liniel & Metzger 2023)

$$t_e \approx \left(\frac{\kappa M_{\text{sh}}}{4\pi c v_{\text{ej}}}\right)^{\frac{1}{2}} \approx 0.18 \frac{r_*}{\alpha_{-1}^{\frac{1}{2}} \dot{m}^{\frac{1}{2}}} \left(\frac{P_1}{M_6}\right)^{\frac{2}{3}} \text{ hr}. \quad (8)$$

3.4. Luminosity

Next, we consider the energy evolution of the shocked matter. The following Eq. (5), the total internal energy of the immediately post-shock matter, which is dominated by radiation, is $E_{i,0} = M_{\text{sh}}v_k^2$. Note that it is on the same order of magnitude as the total kinetic energy of the shocked matter $E_k = \frac{1}{2}M_{\text{sh}}v_k^2$ (Liniel & Metzger 2023).

During expansion, the temperature of the shocked matter decreases and a large fraction of the internal energy is converted into the expansion kinetic energy of the shocked matter. With $\gamma = \frac{4}{3}$, the internal energy evolves with the volume as $E_i \propto V^{1-\gamma}$. So, the internal energy of the shocked matter at R_{diff} is

$$\begin{aligned} E_i(R_{\text{diff}}) &= E_{i,0} \times \left(\frac{2\pi R_*^2 h/7}{\frac{4\pi}{3} R_{\text{diff}}^3}\right)^{\frac{1}{3}} \\ &= 3.5 \times 10^{44} r_*^{\frac{5}{3}} \dot{m}^{-\frac{1}{6}} \alpha_{-1}^{-\frac{1}{2}} M_6^{\frac{1}{3}} \text{ erg/s}. \end{aligned} \quad (9)$$

Note that the factor of $\frac{1}{7}$ in the numerator of the second equation comes from the shock compression during collision. Therefore, the peak luminosity of the diffusive radiation from the expanding shocked matter is

$$L_{\text{p}} = \frac{E_i(R_{\text{diff}})}{t_e} = 5.5 \times 10^{41} M_6 \left(\frac{r_*}{P_1}\right)^{\frac{2}{3}} \dot{m}^{\frac{1}{3}} \text{ erg/s}. \quad (10)$$

Note that it does not depend on Σ_{d} , thus the parameter α vanishes.

3.5. The Quiescent-level Accretion

The quiescent-level X-ray flux between two neighboring eruptions can be considered to be emitted from the inner region of the accretion disk. Assuming the accretion rate during the quiescent state is not much different from that during the collision, one can write the quiescent-level luminosity as

$$L_Q = 1.5 \times 10^{43} \eta_{-1} M_6 \dot{m} \text{ erg/s}, \quad (11)$$

where $\eta = 0.1 \times \eta_{-1}$ is the radiative efficiency.

3.6. Infer r_* from Observables

Eqs. (8), (10) and (11) give the three observables (t_{PQE} , L_p and L_Q) from the star-disk collision model. Here, we attempt to investigate what r_* is allowed or required by the model to satisfy these observables.

Notice that α and η are the two fudge “factors” that describe the working mechanism of the accretion disk, and \dot{m} is one of the disk properties; all others are observable, or measurable in principle. One can get rid of \dot{m} and express r_* in terms of observables in two ways. First, one can infer \dot{m} from Eq. (10), and plug it into Eq. (8) to get

$$r_* = 3.7 L_{p,42}^{\frac{3}{4}} P_1^{\frac{1}{6}} M_6^{-\frac{5}{12}} \left(\frac{t_e}{1 \text{ hr}} \right)^{\frac{1}{2}} \alpha_{-1}^{\frac{1}{4}}. \quad (12)$$

Secondly, we can obtain \dot{m} from L_Q (Eq. 11) and plug it into Eq. (10), to get

$$r_* = 28 L_{p,42}^{\frac{3}{2}} L_{Q,41}^{-\frac{1}{2}} \frac{P_1}{M_6} \eta_{-1}^{\frac{1}{2}}, \quad (13)$$

where $L_{Q,41} = L_Q / (10^{41} \text{ erg/s})$ and $L_{p,42} = L_p / (10^{42} \text{ erg/s})$. In this way, we obtain two constraints on r_* , both of which must be satisfied, and each contains one fudge factor only.

3.7. Radiation Temperature

One could also estimate the color temperature T_p of the radiation from the shocked material as another key observable.

When the star-disk collision occurs, the material shocked by the collision will be radiation-dominated and optically thick. Firstly, the radiation energy density is expressed as $u_\gamma = L_p / [4\pi R_{\text{diff}}^2 v_{ej}]$ (Linial & Metzger 2023). Secondly, assuming that the radiation of QPEs is dominated by blackbody radiation, $u_\gamma = aT_p^4$, where a is the radiation constant, then T_p can be expressed in terms of various observables as (also see Linial & Metzger 2023)

$$\begin{aligned} kT_p &= k \left(\frac{u_\gamma}{a} \right)^{\frac{1}{4}} \\ &= 9 L_{p,42}^{\frac{1}{4}} \left(\frac{t_e}{1 \text{ hr}} \right)^{-\frac{1}{2}} P_1^{\frac{1}{4}} M_6^{-\frac{1}{4}} \text{ eV}, \end{aligned} \quad (14)$$

where k is the Boltzmann constant.

Note that Linial & Metzger (2023) argue that if the radiation is not in thermal equilibrium with the matter at R_{diff} , then kT_p might be higher.

3.8. Constraint from Stellar Tidal Disruption

Now we consider another constraint on r_* . The stellar orbit must be sufficiently wide; otherwise the star would be tidally disrupted. A critical orbital radius is the so-called tidal disruption radius (e.g., Rees 1988)

$$R_t = R_* \left(\frac{M_h}{M_*} \right)^{\frac{1}{3}} = 47 r_* M_6^{-\frac{2}{3}} m_*^{-\frac{1}{3}} R_g. \quad (15)$$

The above constraint requires that $R > nR_t$, where $n = 1$ corresponds to the full disruption and $n = 2$ corresponds to the starting point of mass transfer; In other words, $1 < n < 2$ corresponds to the partial disruption of the star.

Plugging Eq. (1) in, this can be rearranged to put a constraint on the stellar radius: $r_* < 2.4 n^{-1} P_1^{\frac{2}{3}} m_*^{\frac{1}{3}}$. Adopting the mass-radius relationship for high-mass zero-age-main-sequence stars $r_* = m_*^{0.6}$ (Kippenhahn et al. 2013), one can rewrite it as

$$r_* < 6.9 n^{-\frac{9}{4}} P_1^{\frac{3}{2}}. \quad (16)$$

4. APPLICATION TO QPE SAMPLE

In this section, for each source, we plot the r_* -constraints as functions of M_h . The numerical range of M_h of an individual source corresponds to the estimate quoted in Sect. 2 and Table. 1.

4.1. GSN 069

We start with the well-known QPE source GSN 069. In Figure 1, we plot the r_* -constraints, Eq. (12) and Eq. (13) as the red and blue lines, respectively. The solid and dashed lines are for two adopted representative values of the unknown parameters (α and η), respectively. The light-purple shadowed region represents the allowed parameter space that could satisfy both Eq. (12) and Eq. (13). The full tidal disruption limit and the partial tidal disruption limit are represented by the green and black horizontal lines, respectively. The region below the green line means that stars with such small r_* can

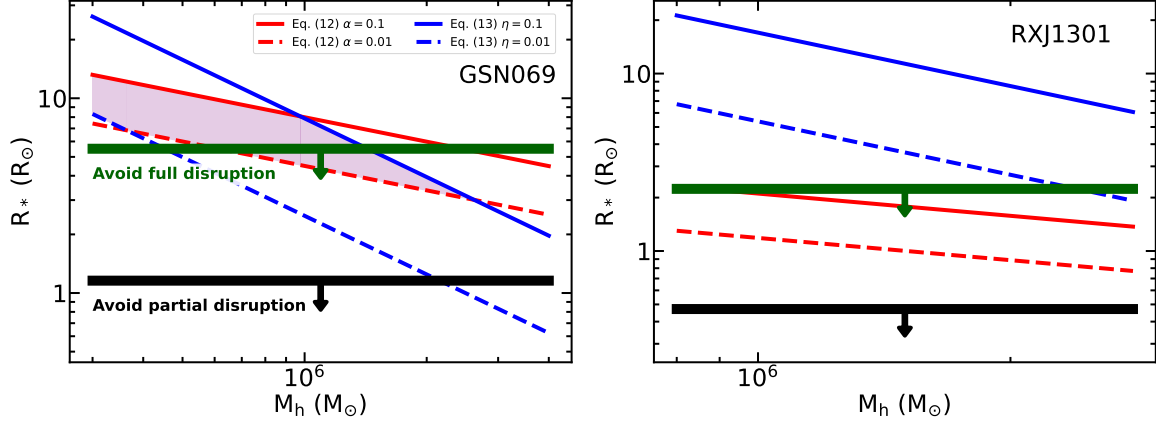


Figure 1. The constraints on the stellar radius for GSN 069 (left panel) and RX J1301 (right panel). The red and blue lines stand for the constraints based on Eq. (12) and Eq. (13), respectively. The solid and dashed lines are for different adopted values of 0.1 and 0.01 for the model parameter (α or η), respectively. The horizontal lines with downward arrows represent the full tidal disruption limit (green, Eq. 16, $n = 1$) and the partial tidal disruption limit (black, Eq. 16, $n = 2$), respectively.

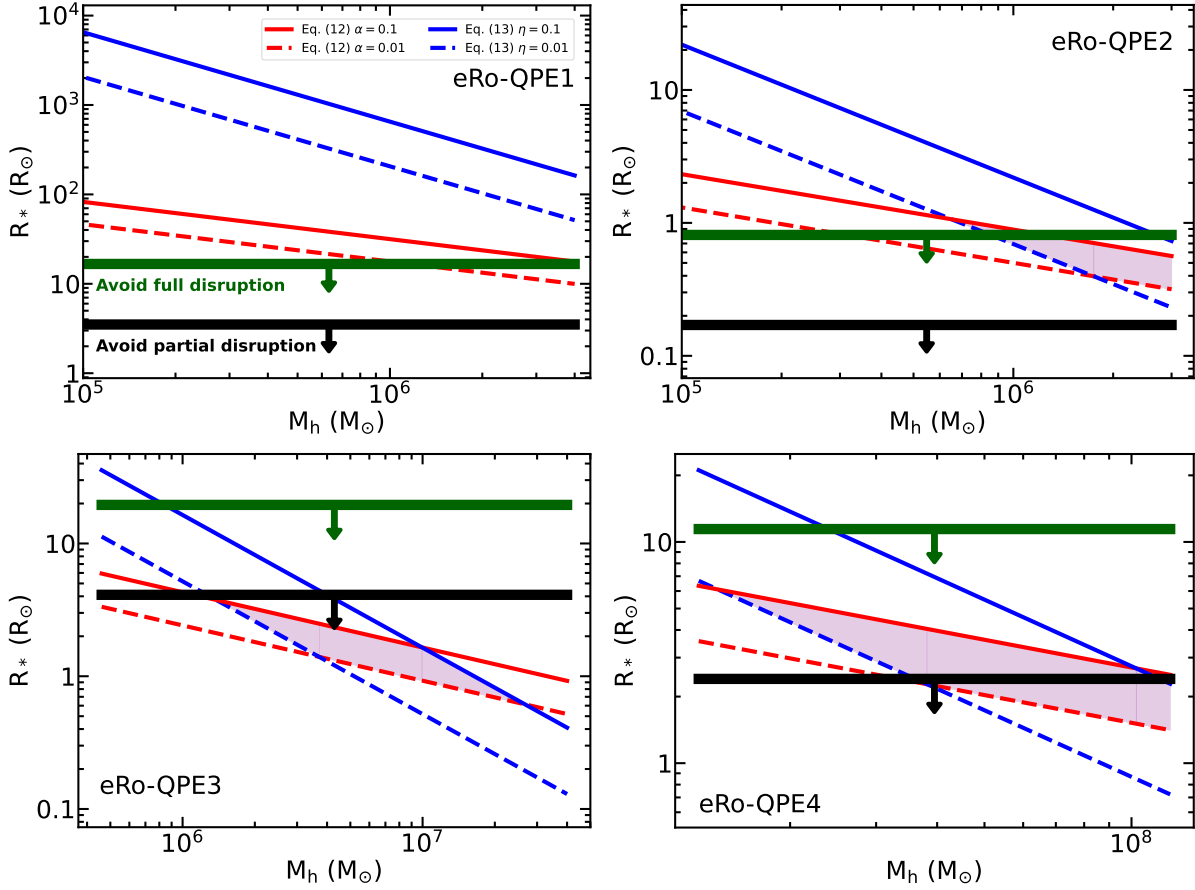


Figure 2. The constraints on the stellar radius for other four QPE sources. The legends are the same as those in the left panel of Figure 1.

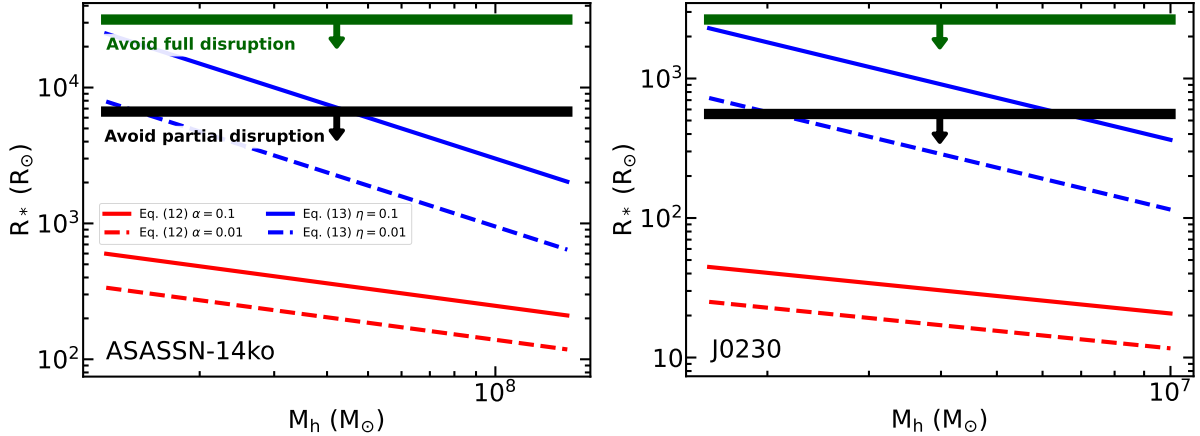


Figure 3. The constraints of stellar radius for longer time-scale repeating sources: ASASSN-14ko and J0230. The legends are the same as those in the left panel of Figure 1.

avoid being tidally disrupted. Similarly, stars with even smaller r_* (below the black line) will not even be tidally stripped.

As the left panel of Figure 1 shows, GSN 069 does have a light-purple shaded region of $r_* \lesssim 10$, especially for $M_h \lesssim 10^6 M_\odot$, that satisfies both constraints. However, most of that region is above the solid green line, meaning that they would have already been tidally disrupted.

Only a small shaded region with small r_* (i.e., below the green solid line) can avoid the full disruption, but they are still well above the black solid line, meaning that they would suffer a significant partial disruption and that disruption would repeat on every orbit. In the latter case, the question arises that whether the stripped mass and its subsequent accretion toward the BH will be the dominant energy source for the observed eruption. Indeed, a few groups have argued for the repeated strippings or mass transfer from a stellar companion as the origin of QPEs (King 2020, 2022, 2023; Zhao et al. 2022; Chen et al. 2023; Wu et al. 2024; Krolik & Linial 2022; Lu & Quataert 2023).

In any case, these results demonstrate that the *simplest* version of the star-disk collision model did not pass our test for GSN 069.

4.2. Other QPE Sources

Next, we present results for other QPE sources. The constraints for RX J1301 are shown in the right panel of Figure 1. It shows that this source does not even have an allowed r_* -parameter space that can satisfy both Eq. (12) and Eq. (13). Considering an extremely low η (e.g., $\sim 10^{-3}$) might allow a light-purple shaded region to appear, but it will still be above the black solid line, meaning that the star would suffer repeated partial disruptions. Therefore, the star-disk model can hardly work for RX J1301.

Figure 2 shows the constraints for other four QPE sources. One can see that for eRo-QPE1, there is no parameter space that satisfies both constraints Eq. (12) and Eq. (13). For eRo-QPE2, a small parameter space of $r_* \sim 0.5$ for $M_h \gtrsim 10^6 M_\odot$ is allowed by both Eq. (12) and Eq. (13), but similar to the situation for GSN 069, it is well above the solid black line, so it will suffer significant partial tidal disruptions.

eRo-QPE3 and eRo-QPE4 fare much better in our test, as were shown in the lower panels of Figure 2. The best case is eRo-QPE3, whose allowed parameter space is $r_* \sim 1$ (i.e., a sun-like star) and $M_h \lesssim 10^7 M_\odot$, and it is free from any tidal stripping. eRo-QPE4 also has an allowed parameter space, and taking into account the tidal stripping limit, that space shrinks to $r_* \sim 2$ and $M_h \sim 10^8 M_\odot$.

4.3. QPE-like Sources with Longer Periods

Now we turn to those QPE-like sources with relatively long periods: ASASSN-14ko and J0230, whose results are shown in Figure 3. Firstly, because these two sources have much longer time scales t_e and P , they require extremely large r_* to power the luminous flares, as can be seen in Eqs. (8) and (10). In some cases, the required r_* (i.e., 10^3 – 10^4 by Eq. 13) is too large to be physically reasonable. Secondly, although a large P – hence a wide orbit – puts such a star safe from a full or partial tidal disruption, there is hardly a common parameter space that can meet both Eqs. (12) and (13). Therefore, the star-disk collision model can be ruled out for these two sources. We note that a repeated partial tidal disruption model has been invoked to explain ASASSN-14ko (Payne et al. 2021, 2022, 2023; Huang et al. 2023) and J0230 (Guolo et al. 2024; Pasham et al. 2024a).

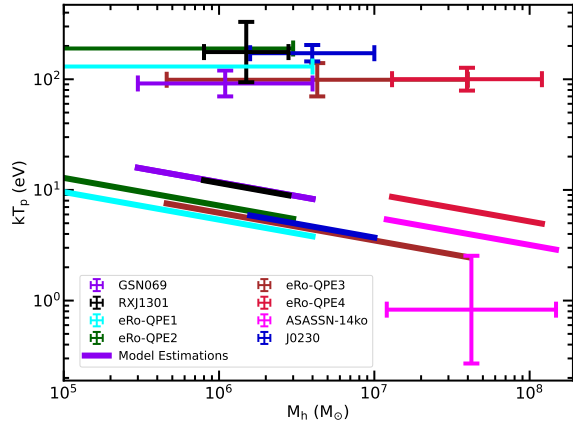


Figure 4. The comparison of the peak radiation temperatures T_p predicted by the star-disk collision model (solid lines) and those observed (crosses with error bars) for the sample. The predicted T_p is calculated from Eq. (14). The horizontal error bars of the observed T_p correspond to the estimated M_h range of each individual source, respectively.

4.4. Comparison of T_p

We also compare the predicted peak radiation temperature T_p (Eq. 14) with the observed ones, which are shown in Figure 4. It is obvious that, except for ASASSN-14ko, the predicted T_p 's for all other sources are one order of magnitude lower than the observed values. This systematic discrepancy poses a serious challenge to the star-disk collision model.

Note that Eq. (14) is based on the assumption that the radiation is fully thermalized with the matter when it is diffusing out of the expanding shocked material. [Linial & Metzger \(2023\)](#) argue that it may not be the case, so that T_p could be higher.

For ASASSN-14ko, the observed $kT_p \sim 1$ eV is low, which is not surprising since its radiation during each eruption is dominated by the optical waveband ([Payne et al. 2021, 2022, 2023; Huang et al. 2023](#)). Thus, the discrepancy does not appear to be an issue. However, we have shown in §4.3 that the star-disk collision model can not pass the r_* test for this source, thus the model can be ruled out.

5. CONCLUSION

The star-disk collision model proposed for QPE and QPE-like sources has attracted a lot of attention and remains a hot topic of discussion. However, the matching between the observed radiative properties, including L_p , t_e and T_p , and the model predictions has not been fully examined. In our study, we derive constraints on r_* and T_p as functions of M_h for the star-disk collision

model, using the typical values of these observables. We then apply this method to a sample of QPE and QPE-like sources, with a particular attention to what value or range of the stellar radius r_* is required to reproduce these observables. The following are our findings.

1) Within our sample, the eruption luminosity and duration constraints require that $r_* \sim 3 - 10$ for GSN 069, $r_* \sim 0.3 - 1$ for eRo-QPE2, $r_* \sim 0.5 - 4$ for eRo-QPE3 and $r_* \sim 2 - 5$ for eRo-QPE4, respectively. There is no allowed parameter space for the rest (RX J1301, eRo-QPE1, ASASSN-14ko and J0230) of the sample.

2) Introducing the full or partial tidal disruption limit further squeezes the allowed parameter space of eRo-QPE4 to $r_* \sim 2$. The best candidate source eRo-QPE3 satisfies this limit well. For GSN 069 and eRo-QPE2, however, they would have suffered significant partial disruption and the accretion of the stripped mass might be the dominant energy source powering the eruptions, thus undermining the foundation of the star-disk collision model.

3) There exists a systematic discrepancy between the model-predicted $T_p \sim (0.01 \text{ keV})$ and observed values $\sim (0.1 \text{ keV})$, though the incomplete thermalization of the diffusive radiation might be a remedy.

Our findings pose serious challenges to the star-disk collision model. Specifically, we find that for most of the sample, the requirements of r_* to reproduce both L_p and t_e , and the requirement that the star should not be partially disrupted, are in tension with each other.

One could also consider a compact object, such as a BH, as the object that collides with the disk. In this case, the eruptions will be produced by the accretion of the material that the BH gravitationally captured during the collision. The gravitational capture radius is $R_c = 2GM_*/v_k^2 \approx 5 \times 10^{-4} m_* P_1^{2/3} M_6^{-2/3} R_\odot$, and the captured mass is $M_c = 2\pi R_c^2 (\sqrt{2}\Sigma_d)$. The total energy released from the accretion is $E_{\text{acc}} = \eta M_c c^2 \approx 4 \times 10^{39} \eta_{-1} \alpha_{-1}^{-1} \dot{m}^{-1} m_*^2 P_1^{7/3} M_6^{-7/3} \text{ erg}$.

The typically observed total radiation energy during one eruption from a QPE source is $E_{\text{rad}} \simeq 7 \times 10^{45} \text{ erg}$ ([Miniutti et al. 2023b](#)). This would require $m_* \sim 10^3$, i.e., an intermediate mass BH, as the collider. Driven by gravitational wave radiation, the orbital decay time scale of this binary massive BH system would be $\tau_{\text{GW}} \approx 2 \times 10^3 (m_*/10^3)^{-1} M_6^{-2/3} P_1^{5/3} \text{ yr}$ ([Shapiro & Teukolsky 1986; Peters & Mathews 1963](#)).

This work is supported by the National Natural Science Foundation of China grant 12393814.

REFERENCES

- Arcodia, R., Merloni, A., Nandra, K., et al. 2021, *Nature*, 592, 704, doi: [10.1038/s41586-021-03394-6](https://doi.org/10.1038/s41586-021-03394-6)
- Arcodia, R., Linial, I., Miniutti, G., et al. 2024a, *A&A*, 690, A80, doi: [10.1051/0004-6361/202451218](https://doi.org/10.1051/0004-6361/202451218)
- Arcodia, R., Liu, Z., Merloni, A., et al. 2024b, *A&A*, 684, A64, doi: [10.1051/0004-6361/202348881](https://doi.org/10.1051/0004-6361/202348881)
- Arnett, W. D. 1980, *ApJ*, 237, 541, doi: [10.1086/157898](https://doi.org/10.1086/157898)
- Chakraborty, J., Arcodia, R., Kara, E., et al. 2024, *ApJ*, 965, 12, doi: [10.3847/1538-4357/ad2941](https://doi.org/10.3847/1538-4357/ad2941)
- Chen, J.-H., Shen, R.-F., & Liu, S.-F. 2023, *ApJ*, 947, 32, doi: [10.3847/1538-4357/acbfb6](https://doi.org/10.3847/1538-4357/acbfb6)
- Dai, L. J., Fuerst, S. V., & Blandford, R. 2010, *MNRAS*, 402, 1614, doi: [10.1111/j.1365-2966.2009.16038.x](https://doi.org/10.1111/j.1365-2966.2009.16038.x)
- Evans, P. A., Nixon, C. J., Campana, S., et al. 2023, *Nature Astronomy*, 7, 1368, doi: [10.1038/s41550-023-02073-y](https://doi.org/10.1038/s41550-023-02073-y)
- Franchini, A., Bonetti, M., Lupi, A., et al. 2023, *A&A*, 675, A100, doi: [10.1051/0004-6361/202346565](https://doi.org/10.1051/0004-6361/202346565)
- Frank, J., King, A., & Raine, D. J. 2002, *Accretion Power in Astrophysics: Third Edition*
- Giustini, M., Miniutti, G., & Saxton, R. D. 2020, *A&A*, 636, L2, doi: [10.1051/0004-6361/202037610](https://doi.org/10.1051/0004-6361/202037610)
- Guolo, M., Pasham, D. R., Zajaček, M., et al. 2024, *Nature Astronomy*, 8, 347, doi: [10.1038/s41550-023-02178-4](https://doi.org/10.1038/s41550-023-02178-4)
- Huang, S., Jiang, N., Shen, R.-F., Wang, T., & Sheng, Z. 2023, *ApJL*, 956, L46, doi: [10.3847/2041-8213/acffc5](https://doi.org/10.3847/2041-8213/acffc5)
- Ingram, A., Motta, S. E., Aigrain, S., & Karastergiou, A. 2021, *MNRAS*, 503, 1703, doi: [10.1093/mnras/stab609](https://doi.org/10.1093/mnras/stab609)
- Kaur, K., Stone, N. C., & Gilbaum, S. 2023, *MNRAS*, 524, 1269, doi: [10.1093/mnras/stad1894](https://doi.org/10.1093/mnras/stad1894)
- King, A. 2020, *MNRAS*, 493, L120, doi: [10.1093/mnrasl/slaa020](https://doi.org/10.1093/mnrasl/slaa020)
- . 2022, *MNRAS*, 515, 4344, doi: [10.1093/mnras/stac1641](https://doi.org/10.1093/mnras/stac1641)
- . 2023, *MNRAS*, 520, L63, doi: [10.1093/mnrasl/sladd006](https://doi.org/10.1093/mnrasl/sladd006)
- Kippenhahn, R., Weigert, A., & Weiss, A. 2013, *Stellar Structure and Evolution*, doi: [10.1007/978-3-642-30304-3](https://doi.org/10.1007/978-3-642-30304-3)
- Krolik, J. H., & Linial, I. 2022, *ApJ*, 941, 24, doi: [10.3847/1538-4357/ac9eb6](https://doi.org/10.3847/1538-4357/ac9eb6)
- Linial, I., & Metzger, B. D. 2023, *ApJ*, 957, 34, doi: [10.3847/1538-4357/acf65b](https://doi.org/10.3847/1538-4357/acf65b)
- Linial, I., & Quataert, E. 2024, *MNRAS*, 527, 4317, doi: [10.1093/mnras/stad3470](https://doi.org/10.1093/mnras/stad3470)
- Linial, I., & Sari, R. 2023, *ApJ*, 945, 86, doi: [10.3847/1538-4357/acbd3d](https://doi.org/10.3847/1538-4357/acbd3d)
- Lu, W., & Quataert, E. 2023, *MNRAS*, 524, 6247, doi: [10.1093/mnras/stad2203](https://doi.org/10.1093/mnras/stad2203)
- Metzger, B. D., Stone, N. C., & Gilbaum, S. 2022, *ApJ*, 926, 101, doi: [10.3847/1538-4357/ac3ee1](https://doi.org/10.3847/1538-4357/ac3ee1)
- Miniutti, G., Giustini, M., Arcodia, R., et al. 2023a, *A&A*, 674, L1, doi: [10.1051/0004-6361/202346653](https://doi.org/10.1051/0004-6361/202346653)
- . 2023b, *A&A*, 670, A93, doi: [10.1051/0004-6361/202244512](https://doi.org/10.1051/0004-6361/202244512)
- Miniutti, G., Saxton, R. D., Giustini, M., et al. 2019, *Nature*, 573, 381, doi: [10.1038/s41586-019-1556-x](https://doi.org/10.1038/s41586-019-1556-x)
- Miniutti, G., Franchini, A., Bonetti, M., et al. 2025, *A&A*, 693, A179, doi: [10.1051/0004-6361/202452400](https://doi.org/10.1051/0004-6361/202452400)
- Pan, X., Li, S.-L., Cao, X., Miniutti, G., & Gu, M. 2022, *ApJL*, 928, L18, doi: [10.3847/2041-8213/ac5faf](https://doi.org/10.3847/2041-8213/ac5faf)
- Pasham, D., Coughlin, E., Nixon, C., et al. 2024a, *arXiv e-prints*, arXiv:2411.05948, doi: [10.48550/arXiv.2411.05948](https://doi.org/10.48550/arXiv.2411.05948)
- Pasham, D., Kejriwal, S., Coughlin, E., et al. 2024b, *arXiv e-prints*, arXiv:2411.00289, doi: [10.48550/arXiv.2411.00289](https://doi.org/10.48550/arXiv.2411.00289)
- Payne, A. V., Shappee, B. J., Hinkle, J. T., et al. 2021, *ApJ*, 910, 125, doi: [10.3847/1538-4357/abe38d](https://doi.org/10.3847/1538-4357/abe38d)
- . 2022, *ApJ*, 926, 142, doi: [10.3847/1538-4357/ac480c](https://doi.org/10.3847/1538-4357/ac480c)
- Payne, A. V., Auchettl, K., Shappee, B. J., et al. 2023, *ApJ*, 951, 134, doi: [10.3847/1538-4357/acd455](https://doi.org/10.3847/1538-4357/acd455)
- Peters, P. C., & Mathews, J. 1963, *Physical Review*, 131, 435, doi: [10.1103/PhysRev.131.435](https://doi.org/10.1103/PhysRev.131.435)
- Pihajoki, P. 2016, *MNRAS*, 457, 1145, doi: [10.1093/mnras/stv3023](https://doi.org/10.1093/mnras/stv3023)
- Raj, A., Nixon, C. J., & Doğan, S. 2021, *ApJ*, 909, 81, doi: [10.3847/1538-4357/abdc24](https://doi.org/10.3847/1538-4357/abdc24)
- Rees, M. J. 1988, *Nature*, 333, 523, doi: [10.1038/333523a0](https://doi.org/10.1038/333523a0)
- Shakura, N. I., & Sunyaev, R. A. 1973, *A&A*, 24, 337
- Shapiro, S. L., & Teukolsky, S. A. 1986, *Black Holes, White Dwarfs and Neutron Stars: The Physics of Compact Objects*
- Śniegowska, M., Grzędzielski, M., Czerny, B., & Janiuk, A. 2023, *A&A*, 672, A19, doi: [10.1051/0004-6361/202243828](https://doi.org/10.1051/0004-6361/202243828)
- Suková, P., Zajaček, M., Witzany, V., & Karas, V. 2021, *ApJ*, 917, 43, doi: [10.3847/1538-4357/ac05c6](https://doi.org/10.3847/1538-4357/ac05c6)
- Sun, L., Shu, X., & Wang, T. 2013, *ApJ*, 768, 167, doi: [10.1088/0004-637X/768/2/167](https://doi.org/10.1088/0004-637X/768/2/167)
- Tagawa, H., & Haiman, Z. 2023, *MNRAS*, 526, 69, doi: [10.1093/mnras/stad2616](https://doi.org/10.1093/mnras/stad2616)
- Vurm, I., Linial, I., & Metzger, B. D. 2024, *arXiv e-prints*, arXiv:2410.05166, doi: [10.48550/arXiv.2410.05166](https://doi.org/10.48550/arXiv.2410.05166)
- Wu, X.-J., Yuan, Y.-F., Luo, Y., & Lin, W. 2024, *MNRAS*, 529, 1440, doi: [10.1093/mnras/stae641](https://doi.org/10.1093/mnras/stae641)
- Xian, J., Zhang, F., Dou, L., He, J., & Shu, X. 2021, *ApJL*, 921, L32, doi: [10.3847/2041-8213/ac31aa](https://doi.org/10.3847/2041-8213/ac31aa)
- Yao, P. Z., Quataert, E., Jiang, Y.-F., Lu, W., & White, C. J. 2025, *ApJ*, 978, 91, doi: [10.3847/1538-4357/ad8911](https://doi.org/10.3847/1538-4357/ad8911)
- Zhao, Z. Y., Wang, Y. Y., Zou, Y. C., Wang, F. Y., & Dai, Z. G. 2022, *A&A*, 661, A55, doi: [10.1051/0004-6361/202142519](https://doi.org/10.1051/0004-6361/202142519)

Zhou, C., Huang, L., Guo, K., Li, Y.-P., & Pan, Z. 2024a,
PhRvD, 109, 103031, doi: [10.1103/PhysRevD.109.103031](https://doi.org/10.1103/PhysRevD.109.103031)
Zhou, C., Zeng, Y., & Pan, Z. 2024b, arXiv e-prints,
arXiv:2411.18046, doi: [10.48550/arXiv.2411.18046](https://doi.org/10.48550/arXiv.2411.18046)

Zhou, C., Zhong, B., Zeng, Y., Huang, L., & Pan, Z. 2024c,
PhRvD, 110, 083019, doi: [10.1103/PhysRevD.110.083019](https://doi.org/10.1103/PhysRevD.110.083019)